(Cell Signaling Technology, Beverly, MA) in PBS-T for 30 min at room temperature. The membranes were washed with PBS-T and then visualized by enhanced chemiluminescence using an ECL Western blotting detection kit (Amersham Biosciences). Western blotting images were obtained with a luminescent image analyzer (LAS-1000, FUJIFILM, Kanagawa, Japan).

2.4 Immunofluorescence experiments

To confirm the localization of FLAG-tagged point mutants, immunofluorescence experiments were performed. Transiently transfected HEK293 cells were fixed with 4% paraformaldehyde for 5 min at room temperature and washed with PBS. Non-specific binding was avoided by the addition of 50% Block Ace (Dainippon Pharmaceutical, Osaka, Japan) and 50% fetal bovine serum. After PBS washing, anti-FLAG antibody (Sigma-Aldrich) in PBS with 0.1% saponin solution was added to the cells. After incubation for 1 h at 37°C, the cells were washed with PBS and then incubated with TRITC-conjugated anti-mouse IgG antibody (Sigma-Aldrich) in PBS with 0.1% saponin solution for 30 min at 37°C. After PBS washing, the stained cells were observed using a confocal laser scanning microscope (FV500, Olympus, Tokyo, Japan).

2.5 Electrophysiological experiments

Prestin-expressing cells exhibit bell-shaped NLC in response to the change of membrane potential[6),(8),(9)]. As NLC shows a voltage-dependent charge transfer of prestin, the anion transport function of prestin was evaluated with NLC measured by the whole-cell patch-clamp technique. For patch-clamp measurements, the transiently transfected HEK293 cells in a culture dish were transferred to several glass-base dishes (IWAKI, Chiba, Japan). Electrodes were pulled from the borosilicate glass tube (TW150-4, World Precision Instruments, Inc., Sarasota, FL) by a programmable pullar (Model P-97, Sutter Instruments Co., Novato, CA), and had resistances between 2 and 5 MΩ. Electrodes were filled with an internal solution with the following composition: 140 mM CsCl, 2 mM $MgCl_2$, 10 mM EGTA and 10 mM HEPES, pH adjusted to 7.2 with CsOH. The external medium had the following composition: 120 mM NaCl, 20 mM TAE-Cl, 2 mM $CoCl_2$, 2 mM $MgCl_2$, 10 mM HEPES and 5 mM glucose, pH adjusted to 7.2 with NaOH.

The measurement system consists of a patch amplifier (Axopatch 200B amplifier, Axon Instruments, Foster City, CA), an A/DD/A converter (Digidata 1320A, Axon Instruments), a personal computer and a function generator (WF1944, NF Electronic Instruments, Kanagawa, Japan). Measurements of membrane capacitance were performed using the "membrane test" feature of pCLAMP 8.0 acquisition software (Axon Instruments). A test square wave (amplitude, 20 mV; period T = 4 msec, i.e., frequency, 250 Hz) was generated by the personal computer controlled by pCLAMP 8.0 software and applied to the cell through the amplifier. The transient current, which is caused by the test square wave, was then sampled through the amplifier. Transient current Q, current decay τ and total resistance R_t were continuously calculated by pCLAMP 8.0 software at a resolution of 25 Hz, by averaging the responses to 10 positive and 10 negative consecutive test steps, and measured values of these parameters were stored in the computer. Access resistance R_a, membrane resistance R_m and membrane capacitance C_m were then obtained by substituting Q, τ and R_t into the following equations[6)]:

$$R_a = \frac{R_t \tau V_c}{Q R_t + \tau V_c}, \tag{1}$$

$$R_m = R_t - R_a, \tag{2}$$

$$C_m = \left(\frac{R_t}{R_m}\right)^2 \frac{Q}{V_c}, \tag{3}$$

where V_c is a voltage step. To determine the voltage dependence of membrane capacitance, triangular voltage ramps were superimposed on the above-mentioned square test wave. This triangular voltage wave (period T = 2 sec) was generated by the function generator and swung the cell potential from −140 mV to +70 mV[12)]. After the measurements, the membrane capacitance was plotted versus the membrane potential.

The membrane capacitance recorded from prestin-expressing cells was fitted to the derivative of the Boltzmann function[5)],

$$C_m(V) = C_{lin} + \frac{Q_{max}}{\alpha e^{\frac{V-V_{1/2}}{\alpha}} \left(1 + e^{-\frac{V-V_{1/2}}{\alpha}}\right)^2}, \tag{4}$$

where C_{lin} is the linear capacitance, Q_{max} is the maximum charge transfer, V is the membrane potential and $V_{1/2}$ is the voltage at half-maximal charge transfer. In Eq. (4), α is the slope factor of the voltage-dependent charge transfer and is given by

$$\alpha = kT/ze, \tag{5}$$

where k is Boltzmann's constant, T is absolute temperature, z is valence and e is electron charge. The software program KaleidaGraph (Synergy Software, Reading, PA) was used for data analysis and curve fitting. To evaluate the expression level of prestin in the unit cell membrane, Q_{max}, which reflects the expression level of prestin in whole cell membrane, was normalized and designated as charge density. The normalization was achieved by division of Q_{max} by C_{lin}, which is proportional to the membrane area of the cells. The unit of charge density is fC/pF.

3. Results

3.1 Expression and molecular weight of the point mutants

Western blotting was performed in order to confirm the expression of FLAG-tagged point mutants and the

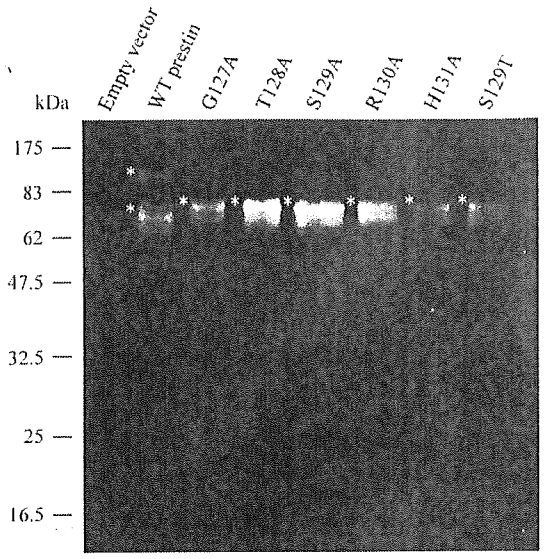

Fig. 5 Results of Western blotting. There was no band in the HEK293 cells transfected with the empty vector. Two major bands of about 100 kDa and 70 kDa were observed in HEK293 cells transfected with FLAG-tagged WT prestin. One major band of about 80 kDa was observed in HEK293 cells transfected with FLAG-tagged point mutants. Asterisks indicate the major bands.

molecular weight of the expressed proteins in HEK293 cells. The results of Western blotting of HEK293 cells transfected separately with an empty vector, FLAG-tagged WT prestin or FLAG-tagged point mutants are shown in Fig. 5. Major bands are indicated by asterisks. There was no band in HEK293 cells transfected with the empty vector. Two major bands of about 100 kDa and 70 kDa were detected in HEK293 cells transfected with FLAG-tagged WT prestin. One major band of about 80 kDa was detected in HEK293 cells transfected with FLAG-tagged point mutants.

3.2 Localization of the point mutants

The localization of FLAG-tagged point mutants in HEK293 cells was examined by immunofluorescence experiments. After confirming the introduction of the expression vectors by GFP observation, cell morphology and TRITC staining was observed. The differential and immunofluorescence images of HEK293 cells separately transfected with the empty vector, FLAG-tagged WT prestin or FLAG-tagged point mutants are shown in Fig. 6. HEK293 cells transfected with the empty vector were not stained. In the case of FLAG-tagged WT prestin and FLAG-tagged point mutants except for T128A, the membrane of transfected cells was stained. By contrast, in the case of FLAG-tagged T128A, both cell membrane and cytoplasm, except for the nucleus, were stained.

3.3 Functional evaluation of the point mutants

To evaluate the anion transport function of the point

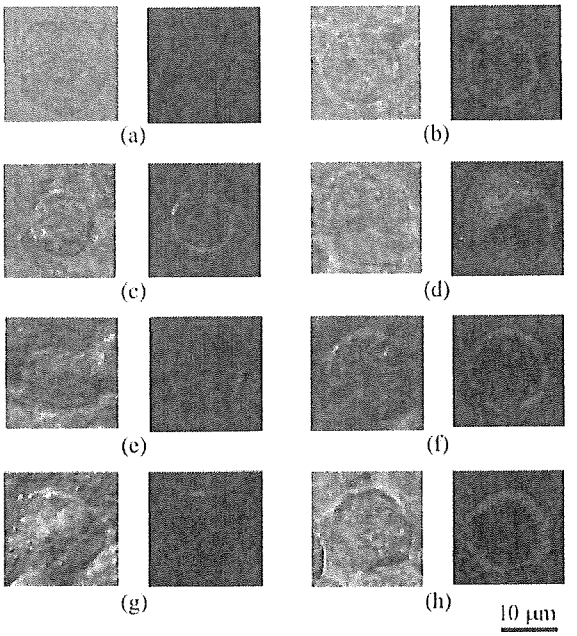

Fig. 6 Differential and immunofluorescence images of HEK293 cells separately transfected with WT prestin or the point mutants. (a) Empty vector. (b) WT prestin. (c) G127A. (d) T128A. (e) S129A. (f) R130A. (g) H131A. (h) S129T. HEK293 cells separately transfected with WT prestin or the point mutants except T128A were stained in the cell membrane. By contrast, HEK293 cells transfected with T128A were stained not only in the cell membrane but also in the cytoplasm.

mutants, whole-cell patch-clamp technique was used. To estimate the NLC of unit cell surface, the normalized nonlinear capacitance $C_{\mathrm{nonlin/lin}}$ was defined as

$$C_{\mathrm{nonlin/lin}}(V)=\frac{C_{\mathrm{nonlin}}}{C_{\mathrm{lin}}}=\frac{(C_{\mathrm{m}}(V)-C_{\mathrm{lin}})}{C_{\mathrm{lin}}}, \qquad (6)$$

where C_{nonlin} is the nonlinear component of the measured membrane capacitance. Furthermore, to compare the normalized data of the point mutants with that of the WT prestin, $C_{\mathrm{nonlin/lin}}(V)$ was divided by the maximum $C_{\mathrm{nonlin/lin}}(V)$ of WT prestin and termed relative $C_{\mathrm{nonlin/lin}}(V)$. Relative $C_{\mathrm{nonlin/lin}}(V)$ plots are shown in Fig. 7. Data points were fitted to Eq. (4), results of the fitting being shown by solid or dashed lines. WT prestin ($n=49$), G127A ($n=6$), T128A ($n=4$), S129A ($n=5$) and R130A ($n=7$) exhibited the NLC versus membrane potential. On the other hand, the membrane capacitance of cells expressing H131A ($n=11$) or S129T ($n=4$) versus membrane potential was constant, similar to the data from the cells transfected with the empty vector. Fitting parameters are shown in Table 2. The charge density, α, and $V_{1/2}$ of the point mutants were compared with that of WT prestin and are shown in Fig. 8. There are statistical differences in charge density between WT prestin and G127A, T128A, S129A or R130A, in α between WT prestin and G127A or R130A and in $V_{1/2}$ between WT prestin and G127A.

Table 2 Fitting parameters for WT prestin and the point mutants

Gene	Charge density (fC/pF)	C_{lin} (pF)	Q_{max} (fC)	α (mV)	$V_{1/2}$ (mV)
WT prestin (n = 49)	20.0 ± 9.6	15.0 ± 5.4	229.6 ± 157.3	30.7 ± 3.7	-62.3 ± 9.2
G127A (n = 6)	7.2 ± 1.2	11.9 ± 1.9	87.6 ± 27.0	43.4 ± 5.0	28.5 ± 11.2
T128A (n = 4)	3.0 ± 1.6	15.0 ± 3.9	47.3 ± 31.3	37.0 ± 6.1	-72.3 ± 10.7
S129A (n = 5)	3.5 ± 1.5	13.4 ± 1.9	47.8 ± 25.1	36.7 ± 5.0	-55.2 ± 15.7
R130A (n = 7)	7.2 ± 6.7	19.4 ± 11.4	114.3 ± 78.5	36.6 ± 5.2	-69.6 ± 11.9

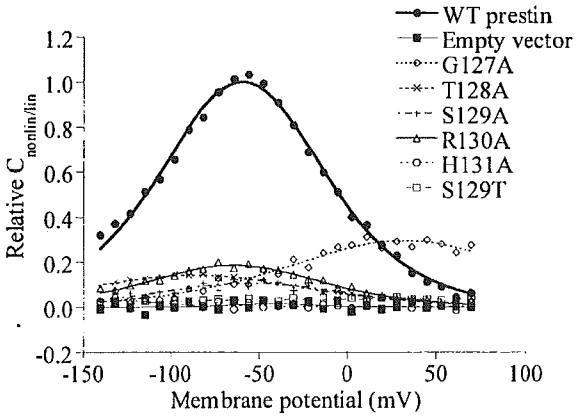

Fig. 7 Representative data of membrane capacitance versus membrane potential. Normalized nonlinear capacitance is divided by the maximum value of the normalized nonlinear capacitance of the WT prestin. Data points were fitted to Eq. (4), which is shown by the solid or dashed lines. WT prestin (n = 49), G127A (n = 6), T128A (n = 4), S129A (n = 5) and R130A (n = 7) exhibited NLC. On the other hand, the empty vector, H131A (n = 11) and S129T (n = 4) did not exhibit it. Fitting parameters for WT prestin were as follows: charge density = 19.3 fC/pF, Q_{max} = 321.6 fC, α = 31.2 mV and $V_{1/2}$ = −59.6 mV; for G127A: charge density = 8.3 fC/pF, Q_{max} = 101.4 fC, α = 45.1 mV and $V_{1/2}$ = 32.0 mV; for T128A: charge density = 3.8 fC/pF, Q_{max} = 58.5 fC, α = 42.1 mV and $V_{1/2}$ = −87.0 mV; for S129A: charge density = 2.4 fC/pF, Q_{max} = 34.5 fC, α = 36.3 mV and $V_{1/2}$ = −54.9 mV; for R130A: charge density = 3.9 fC/pF, Q_{max} = 66.1 fC, α = 33.6 mV and $V_{1/2}$ = −64.2 mV.

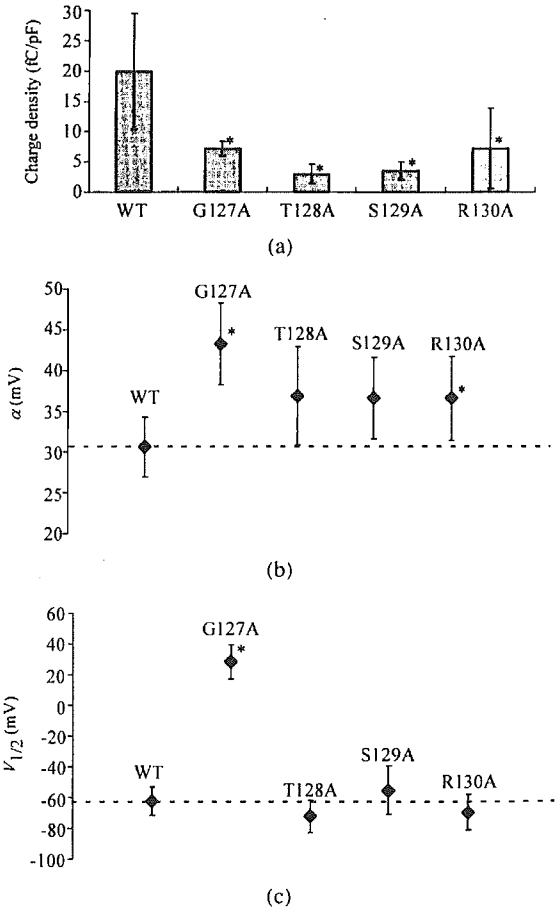

Fig. 8 Fitting parameter variation for the point mutants. (a) Charge density of WT prestin and the point mutants. The charge densities of all point mutants were lower than that of WT prestin, and there was a statistical difference. (b) α of WT prestin and the point mutants. There was a statistical difference between α of WT prestin and those of the G127A and the R130A. (c) $V_{1/2}$ of WT prestin and the point mutants. Only G127A displayed a statistical significant shift of $V_{1/2}$ to the depolarizing side. Asterisks represent significance vs. WT prestin ($p < 0.05$).

4. Discussion

As shown in Fig. 5, no band appeared in the HEK293 cells transfected with the empty vector. This result suggests that the band which appeared in the other transfected cells showed only prestin. The theoretical molecular weights of FLAG-tagged WT prestin and FLAG-tagged point mutants are 84.6 kDa. However, the results of Western blotting show two major bands of about 100 kDa and 70 kDa in the cells transfected with WT prestin as shown in Fig. 5. In general, there are two major types of N-linked carbohydrates: complex oligosaccharides and high-mannose oligosaccharides. It is considered that the 100 kDa band detected in the presnt study indicates prestin glycosylated with complex-type oligosaccharides and the 70 kDa band indicates prestin glycosylated

with high-mannose-type oligosaccharides and unglycosylated prestin. The broadness of the band detected around 100 kDa is considered to be due to the variation in the size of carbohydrate chains. On the other hand, the band detected around 70 kDa was also broad. As the molecular mass of prestin glycosylated with high-mannose-type oligosaccharides is close to that of unglycosylated prestin, two bands of these proteins may overlap. As a result, the band detected around 70 kDa may be broad. It has been reported that one gycosylated prestin band of about 106 kDa in WT prestin-expressing TSA201 cells, which are derivatives of the HEK293 cell line, was observed and that the band shifted from about 106 kDa to about 72 kDa after deglycosylation, suggesting 72 kDa of unglycosylated prestin[13]. Our results agree with the previous report.

An unglycosylated prestin band appeared at a position lower than the theoretical molecular weight. This result is possibly attributable to the high content of hydrophobic amino acid residues in the membrane protein. More negatively charged sodium dodecyl sulphate (SDS) binds to the hydrophobic amino acids residues of membrane proteins than average soluble proteins and this complex was pulled toward the positive electrode, resulting in faster gel migration.

One major band of about 80 kDa was observed in the cells transfected with the point mutants. The 80 kDa bands of the point mutants as well as the 70 kDa band of WT prestin may indicate prestin glycosylated with high-mannose-type oligosaccharides and unglycosylated prestin. The reason why the feature of the band of the point mutants is different from that of the 70 kDa band of WT prestin may be the difference between the expression level of prestin glycosylated with high-mannose-type oligosaccharides and that of unglycosylated prestin, i.e., cells transfected with WT prestin expressed unglycosylated prestin more than prestin glycosylated with high-mannose-type oligosaccharides and vice versa in the cells transfected with the point mutants.

As shown in Fig. 6, in the results of immunofluorescence experiments, TRITC staining was not observed in HEK293 cells transfected with the empty vector. This result suggests that anti-FLAG antibody recognized only prestin. Hence, the results of immunofluorescence experiments showed that G127A, S129A, R130A, H131A and S129T were expressed in the cell membrane as WT prestin and that T128A was expressed in both the cell membrane and the cytoplasm. As the substitution of alanine for threonine is least likely to disturb the protein structure[14], the change of the localization of T128A is not thought to have been due to the misfolding of T128A. This implies that Thr-128 may play a crucial role in the membrane targeting process. By contrast, the substitution of alanine for glycine, serine, arginine and histidine did not affect this process.

In the whole-cell patch-clamp technique, NLC was not obtained from HEK293 cells transfected with H131A. This result means that H131A lost the anion transport function in HEK293 cells. Bordo and Argos reported that a disturbance of the protein fold possibly occurs due to the substitution of any other amino acid for histidine[14]. This may suggest that histidine is an amino acid which is essential for maintaining any protein structure. Hence, the loss of the anion transport function of H131A may suggest that His-131 is important for protein folding in prestin as well as in other proteins.

In the case of pendrin, substitution of threonine for serine in the GTSRH sequence has been found to cause syndromic hearing impairment[11]. To reveal the effect of the substitution of threonine for serine in the GTSRH sequence on the characteristics of prestin, not only alanine but also threonine was substituted for Ser-129. NLC was not obtained from HEK293 cells transfected with S129T, i.e., S129T lost its anion transport function in HEK293 cells. The difference between serine and threonine is only the presence of an extra methyl group in threonine. Due to the presence of this group, position 129 of prestin sterically excludes threonine. Furthermore, although the NLC was obtained from HEK293 cells transfected with S129A, the charge density was less than that of WT prestin. The charge density reflects the amount of charge transfer in the unit cell surface. The reduction of the charge density of the point mutant was the result of a decrease in the number of functional prestin molecules at the unit cell membrane or a decline in the amount of charge transfer by unit prestin. The only difference between serine and alanine is the presence of the hydroxyl group in serine. It was therefore considered that the hydroxyl group of serine is essential for the anion transport function of prestin or maintaining its structure.

As is the case with S129A, although the NLC was obtained from HEK293 cells separately transfected with G127A, T128A or R130A, the charge density of these mutants was less than that of WT prestin. Since the substitution of alanine for glycine was expected to maintain the protein fold, the reduction of the charge density might not be due to the misfolding of G127A. There were statistical differences in α and $V_{1/2}$ between WT prestin and G127A. The α is a slope factor which characterizes voltage-dependent membrane capacitance and also shows the properties of the anion binding and transport[15]. The larger value of α shows that a larger potential change is necessary for anion binding and for translocating anions across a cell membrane. The $V_{1/2}$ is the voltage at which charges are moved with the smallest voltage-increment. The shift of $V_{1/2}$ indicates that the point changes at which prestin is sensitive for the membrane potential. The α of G127A was significantly larger than that of WT prestin

and the $V_{1/2}$ of G127A was remarkably shifted in the depolarization direction. These results suggest that Gly-127 is associated with anion binding and transport. Furthermore, a multiple amino acid sequence alignment of eleven proteins of the SLC26 family showed that Gly-127 is conserved in all proteins of the SLC26 family, although other amino acids in the GTSRH sequence are conserved in six to eight proteins of this family. This fact also supports the idea that Gly-127 is critical for anion binding and transport of prestin.

Although WT prestin is a membrane protein which transport anions via the cell membrane, prestin expressed in cytoplasm cannot sense the change of membrane potential and cannot transport anions via the cell membrane. In Thr-128, as T128A was expressed in both the cell membrane and cytoplasm, the reduction of its charge density may be due to the decrease in the number of functional prestin molecules at the unit cell membrane. In Arg-130, since it is conceivable that the substitution of alanine for arginine does not maintain the protein structure[14], the reduction of charge density of the R130A is possibly due to R130A being in a misfolded state. However, as R130A exhibits NLC, the degree of misfolding is not as serious as that of H131A.

5. Conclusion

To reveal the role of the GTSRH sequence of prestin at positions 127–131 in the characteristics of prestin, mutational analysis was performed. The results show that the GTSRH sequence plays an important role in the localization of prestin, as well as in its anion transport function.

Acknowledgments

This work was supported by a grant from the Human Frontier Science Program, by a Health and Labour Science Research Grant from the Ministry of Health, Labour and Welfare of Japan, and by Grant-in-Aid for Scientific Research on Priority Areas 15086202 from the Ministry of Education, Culture, Sports, Science and Technology of Japan.

References

(1) Brownell, W.E., Basder, D. and Ribaupierre, Y., Evoked Mechanical Responses of Isolated Cochlear Outer Hair Cells, Science, Vol.227 (1985), pp.94–196.

(2) Kachar, B., Brownell, W.E., Altschuler, R. and Fex, J., Electrokinetic Shape Changes of Cochlear Outer Hair Cells, Nature, Vol.322 (1986), pp.365–368.

(3) Ashmore, J.F., A Fast Motile Response in Guinea-Pig Outer Hair Cells: The Cellular Basis of the Cochlear Amplifier, J. Physiol., Vol.388 (1987), pp.323–347.

(4) Dallos, P., The Active Cochlea, J. Neurosci., Vol.12 (1992), pp.4575–4585.

(5) Santos-Sacchi, J., Reversible Inhibition of Voltage-Dependent Outer Hair Cell Motility and Capacitance, J. Neurosci., Vol.11 (1991), pp.3096–3110.

(6) Huang, G. and Santos-Sacchi, J., Mapping of the Distribution of the Outer Hair Cell Motility Voltage Sensor by Electrical Amputation, Biophys. J., Vol.65 (1993), pp.2228–2236.

(7) Forge, A., Structural Feature of the Lateral Walls in Mammalian Cochlea Outer Hair Cells, Cell Tissue Res., Vol.265 (1991), pp.473–485.

(8) Zheng, J., Shen, W., He, D.Z.Z., Long, K.B., Madison, L.D. and Dallos, P., Prestin Is the Motor Protein of Cochlear Outer Hair Cells, Nature, Vol.405 (2000), pp.149–155.

(9) Ludwjg, J., Oliver, D., Frank, G., Klöcker, N., Gummer, A.W. and Fakler, B., Reciprocal Electromechanical Properties of Rat Prestin: The Motor Molecule from Rat Outer Hair Cells, Proc. Natl. Acad. Sci. U.S.A., Vol.98 (2001), pp.4178–4183.

(10) Liberman, M.C., Gao, J., He, D.Z.Z., Wu, X., Jia, S. and Zuo, J., Prestin Is Required for Electromotility of the Outer Hair Cell and for the Cochlear Amplifier, Nature, Vol.419 (2002), pp.300–304.

(11) Fugazzola, I., Cerutti, N., Mannavola, D., Crino, A., Gasparoni, P., Vannucchi, G. and Beck-Peccoz, P., Differential Diagnosis between Pendred and Pseudo-Pendred Syndromes: Clinical, Radiologic, and Molecular Studies, Pediatr. Res., Vol.51 (2002), pp.479–484.

(12) Frolenkov, G.I., Mammano, F., Belyantseva, I.A., Coling, D. and Kachar, B., Two Distinct Ca^{2+}-Dependent Signaling Pathways Regulate the Motor Output of Cochlear Outer Hair Cells, J. Neurosci., Vol.20 (2000), pp.5940–5948.

(13) Matsuda, K., Zheng, J., Du, G.G., Klocker, N., Madison, L.D. and Dallos, P., N-Linked Glycosylation Sites of the Motor Protein Prestin: Effects on Membrane Targeting and Electrophysiological Function, J. Neurochem., Vol.89 (2004), pp.928–938.

(14) Bordo, D. and Argos, P., Suggestions for "Safe" Residue Substitutions in Site-Directed Mutagenesis, J. Mol. Bio., Vol.217 (1991), pp.721–729.

(15) Oliver, D., He, D.Z.Z., Klöcker, N., Ludwig, J., Schulte, U., Waldegger, S., Ruppersberg, J.P., Dallos, P. and Bernd, F., Intracellular Anions as the Voltage Sensor of Prestin, the Outer Hair Cell Motor Protein, Science, Vol.292 (2001), pp.2340–2343.

(16) Zheng, J., Long, K.B., Shen, W., Madison, L.D. and Dallos, P., Prestin Topology: Localization of Protein Epitopes in Relation to the Plasma Membrane, Neuroreport, Vol.12 (2001), pp.1929–1935.

Relationship between Fluorescence Intensity of GFP and the Expression Level of Prestin in a Prestin-Expressing Chinese Hamster Ovary Cell Line*

Koji IIDA**, Tomoyuki NAGAOKA**, Kouhei TSUMOTO***, Katsuhisa IKEDA****, Izumi KUMAGAI***, Toshimitsu KOBAYASHI† and Hiroshi WADA**

Outer hair cells (OHCs) in mammals can elongate and contract at frequencies up to 100 kHz in response to changes in their membrane potential. The origin of this unique motility is the motor protein prestin, which is densely packed in the lateral membrane of the OHCs. In a previous work, we constructed a prestin-expressing cell line using Chinese hamster ovary (CHO) cells to obtain a stable supply of prestin. When we research prestin using constructed cells, it is necessary to estimate the expression level of prestin in the cells easily and non-invasively. As the prestin gene and a green fluorescent protein (GFP) gene were introduced into constructed cells using the same vector, the expression level of prestin and fluorescence intensity of GFP are possibly correlated. Since this correlation is not clear, however, in this study, we therefore investigated whether the expression level of prestin evaluated by patch-clamp recording and the fluorescence intensity of GFP obtained from fluorescence images are correlated or not. As a result, it was demonstrated that they were correlated. The expression level of prestin can therefore be evaluated by measuring the fluorescence intensity of GFP.

Key Words: Acoustic, Biomechanics, Measurement, Sound, Prestin, Green Fluorescent Protein, Chinese Hamster Ovary Cell, Outer Hair Cell, Patch Clamp Technique

1. Introduction

The high sensitivity and sharp tuning of mammalian hearing originates from a mechanical amplification mechanism known as the 'Cochlear amplifier'[1] (Fig. 1). The outer hair cells (OHCs) in the organ of Corti, which alter their longitudinal length in response to changes in their membrane potential, are involved in this mechanism. This unique type of cell motility, called 'electromotility'[2]-[6], operates at frequencies up to 100 kHz and does not require ATP hydrolysis[7]. The molecular mechanism of electromotility is thought to be a voltage-dependent conformational change of a motor protein densely embedded in the lateral membrane of the OHCs[8] (Fig. 2).

In 2000, this motor protein was identified by a cDNA library subtraction procedure and termed prestin[9]. Since its identification, prestin has been researched intensively to understand its function. Cultured kidney cells transfected with prestin cDNA were found to show voltage-dependent membrane capacitance[9],[10] and electrically evoked changes in cell shape[9], similar to OHCs. The importance of prestin for the auditory mechanism was demonstrated by the fact that prestin knock-out mice exhibited a loss of outer hair cell electromotility in vitro and a significantly elevated hearing threshold of 40–60 dB in vivo[11].

For further explication of the function of prestin, it is necessary to study prestin at the molecular level. As a springboard for such study, access to a stable supply of prestin is essential. For this reason, we constructed a prestin-expressing Chinese hamster ovary (CHO) cell line and confirmed that the constructed cells expressed

* Received 24th May, 2004 (No. 04-4125)
** Department of Bioengineering and Robotics, Tohoku University, 6–6–01 Aoba-yama, Sendai 980–8579, Japan
*** Department of Biomolecular Engineering, Tohoku University, 6–6–07 Aoba-yama, Sendai 980–8579, Japan
**** Department of Otorhinolaryngology, Juntendo University School of Medicine, 2–1–1 Hongo, Bunkyo-ku, Tokyo 113–8431, Japan
† Department of Otolaryngology—Head and Neck Surgery, Tohoku University School of Medicine, 1–1 Seiryo-machi, Sendai 980–8575, Japan.
E-mail: iida@wadalab.mech.tohoku.ac.jp

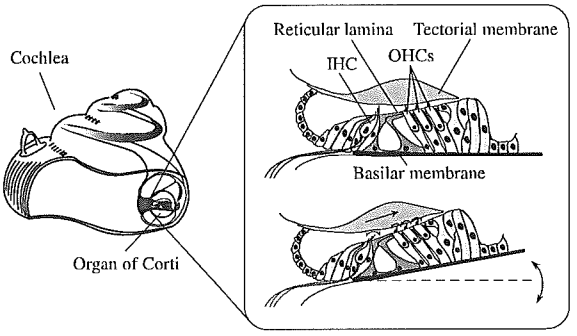

Fig. 1 A schematic of the cochlea and a cross section of the organ of Corti. When the basilar membrane vibrates, shear motion occurs between the reticular lamina and the tectorial membrane. The stereocilia of the IHC and OHCs are deflected by this shear motion, and ions flow into the cells, resulting in intracellular depolarization which causes auditory nerve fiber activation in the IHC. Simultaneously, the OHCs show a motile response and apply force to the basilar membrane.

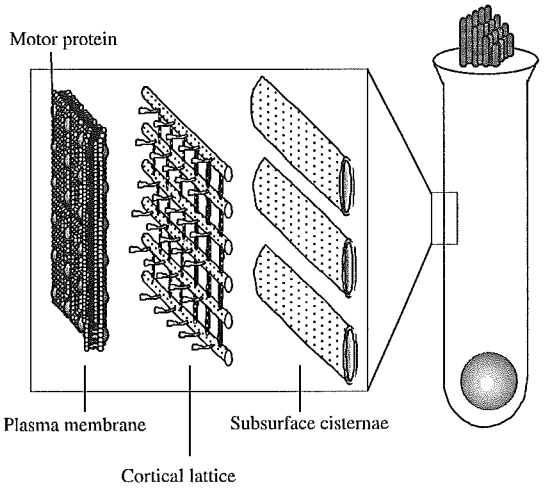

Fig. 2 Lateral wall of the OHC[12]. The OHC lateral wall consists of three layers: plasma membrane, cortical lattice and subsurface cisternae. The motor protein is believed to be embedded in the plasma membrane.

prestin in their plasma membrane and exhibited prestin-originated voltage-dependent nonlinear membrane capacitance[12]. With this cell line, we can obtain prestin-expressing cells anytime without killing animals.

Generally, proteins are expressed and resolved dynamically in a living cell, and each cell has a different cycle of protein expression. As a result, the expression level of prestin in constructed cells may change with time and differ among cells. An indicator of the expression level of prestin in constructed cells is therefore required. The expression level of prestin in prestin-expressing cells is usually determined by analyzing the voltage-dependent nonlinear membrane capacitance, which is derived from a conformational change of prestin, using the whole-cell

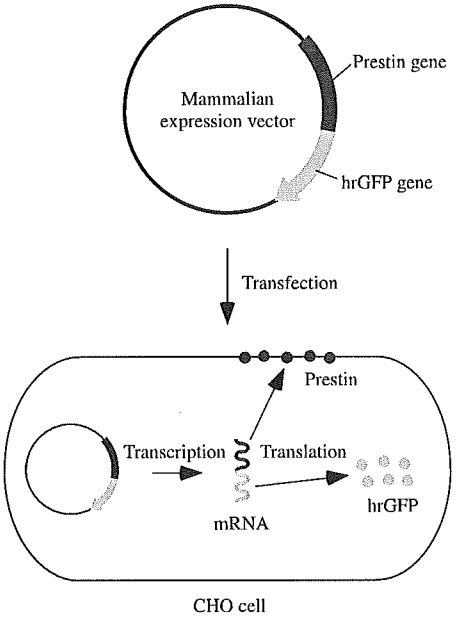

Fig. 3 A schematic of the expression of hrGFP and prestin in a CHO cell. When we constructed a prestin-expressing CHO cell line, the prestin gene and the hrGFP gene were transfected into CHO cells using a mammalian expression vector. In CHO cells, the prestin gene and the hrGFP gene are transcribed into sequential mRNA. Prestin and hrGFP are then translated from this mRNA and localized to the plasma membrane and the cytoplasm of the cell, respectively.

patch-clamp recording technique. However, the procedure of such recording is complicated and requires making an injurious hole in the cell membrane. It is therefore necessary to develop a method by which the expression level of prestin in each cell can be easily and non-invasively investigated.

In the construction of a prestin-expressing CHO cell line in our previous study[12], the prestin gene was transfected into CHO cells using a mammalian expression vector. The humanized *Renilla reniformis* green fluorescent protein (hrGFP) gene, which is a subspecies of the green fluorescent protein (GFP) gene, was inserted as a marker in the vector to confirm the expression of prestin in the cell. GFP is widely used as a marker protein because it yields a green fluorescence, whose intensity is proportional to the amount of GFP, when it is exposed to blue light[13]. When the vector is transfected into CHO cells, the prestin gene and the hrGFP gene are transcribed into sequential mRNA. Prestin and hrGFP are then translated from this mRNA and are localized to the plasma membrane and the cytoplasm of the cell, respectively (Fig. 3). As the prestin gene and the hrGFP gene are transcribed into the same mRNA, the expression level of prestin and fluorescence intensity of hrGFP are possibly correlated. If they do have a correlation, the expression level of prestin

can be evaluated by the fluorescence intensity of hrGFP. However, this correlation has not been clarified yet.

In this study, an attempt was therefore made to determine the relationship between the fluorescence intensity of hrGFP and the expression level of prestin. The fluorescence intensity of hrGFP and the expression level of prestin were evaluated using fluorescence micrographs and whole-cell patch-clamp recordings, respectively.

2. Materials and Methods

2.1 Cell preparation

A prestin-expressing CHO cell line, cultured in flasks with RPMI-1640 medium containing 10% fetal bovine serum, 100 units/mL penicillin and 100 μg/mL streptomycin at 37°C with 5% CO_2, was used. This cell line had been previously constructed[12]. When the prestin gene was transfected into CHO cells, the mammalian expression vector pIRES-hrGFP-1a (Stratagene, La Jolla, CA) was used. In the constructed cells, prestin-coding and hrGFP-coding sequences of the vector are transcribed into the same mRNA. Prestin and hrGFP are then independently translated from this mRNA and are localized in the plasma membrane and the cytoplasm of the cell, respectively.

To transfer the cells to an experimental chamber, they were detached from the flasks by incubating them with 100 μM EDTA in PBS solution for 5–10 min. The EDTA/PBS solution containing CHO cells was then transferred to a conical tube and centrifuged at $250 \times g$ for 5 min. After centrifugation, all of the supernatant was removed, and the cell pellet was resuspended in culture medium. This medium containing the cells was plated on a glass base dish, i.e., the experimental chamber, and incubated for 2–15 hours at 37°C with 5% CO_2 for cell adhesion to the base of the dish. After the incubation, the medium was replaced by an external solution composed of 145 mM NaCl, 5.8 mM KCl, 1.3 mM $CaCl_2$, 0.9 mM $MgCl_2$, 10 mM HEPES, 0.7 mM Na_2HPO_4 and 5.6 mM glucose, adjusted to pH 7.3, and the prepared samples were then used for the following experiment.

2.2 Quantification of hrGFP fluorescence intensity

2.2.1 System for measuring fluorescence intensity

The hrGFP fluorescence intensity of prestin-expressing CHO cells was quantified using the following system (Fig. 4). Samples were observed using an inverted microscope (TE300, Nikon, Tokyo, Japan) with a filter cube (a excitation filter for wavelengths of 450–490 nm, a dichroic mirror for wavelengths of 505 nm or more and a emission filter for wavelengths of 520 nm or more). All of the optical components of the microscope, such as a mercury lamp, filters, iris diaphragms and lenses, were kept under the same conditions during the measurements. Micrographs were detected by a black and white CCD camera (C2400-77, Hamamatsu Photonics, Shizuoka, Japan) with

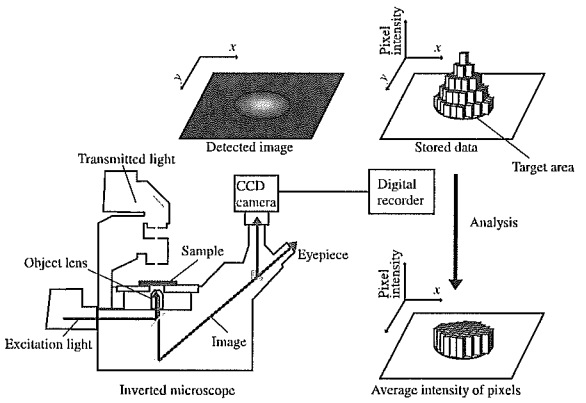

Fig. 4 Measurement system of hrGFP fluorescence intensity. Samples were observed using an inverted microscope. Images were detected by CCD camera, and signals of images were continuously transmitted to a digital recorder. One frame of the transmitted signals was stored in the digital recorder as a static image. The average intensity of pixels in the target area in the stored image was calculated using Eq. (1).

a contrast gain of 10.0, image signals being transmitted to a digital recorder (DCR-PC110, Sony, Tokyo, Japan) at 30 frames per second. One frame of the transmitted signals was stored in the digital recorder as a static image at a resolution of 640 × 480 pixels with 256 levels. The stored images were analyzed using the histogram function of Adobe Photoshop image processing software (Adobe systems, San Jose, CA). The average intensity of pixels in the target area was calculated using the following equation:

$$\text{Average intensity} = \frac{\sum_{i=1}^{n} I_i}{n}, \tag{1}$$

where n is the number of pixels included in the target area and I_i is the intensity of the ith pixel.

Before evaluation of the hrGFP fluorescence intensity of the constructed cells, the relationship between the intensity of the light entering the object lens and the obtained pixel intensity was calibrated within the range of hrGFP fluorescence intensity. Transmitted light for bright field observation, the output voltage of which was fixed, was used as incoming light. Incoming light intensity was altered by passing the transmitted light through neutral density (ND) filters (Olympus, Tokyo, Japan) located on a stage. The relative light intensity in the absence of a filter was defined as 100%, and intensities with ND50, ND25, ND12 and ND6 filters were defined as 50%, 25%, 12% and 6%, respectively. When light was completely shielded, relative incoming light intensity was defined as 0%. The filter cube was used to obtain images. The same range of wavelengths as that of the hrGFP fluorescence is included in the transmitted light and is detected by the CCD camera. Images were taken of the respective in-

coming light intensities. The obtained average intensity of pixels within the area, corresponding to a circle with a diameter of 20 μm located in the center of the image, was calculated using Eq. (1) and plotted against relative incoming light intensities controlled by the ND filters. Measurements were made in a dark room and room temperature was maintained at 23–25°C through out the experiment.

2.2.2 Quantification of hrGFP fluorescence intensity of prestin-expressing CHO cells After replacement of the medium by the external solution, prestin-expressing CHO cells plated on the experimental chamber were observed using the microscope under exposure of excitation light at a wave length of 450–490 nm to detect brightly fluorescent cells with spherical shape. The focus plane was set at the center of a target cell. The fluorescence image of the cell was then stored as mentioned above. Furthermore, a bright field image was taken under white light exposure in the same area as that of the fluorescence image.

To obtain the hrGFP fluorescence intensity of a cell, first, the outline of the target cell was determined from the bright field image. Next, in the fluorescence image, the average intensity of pixels within the determined outline of the target cell was calculated (Fig. 5). The obtained value represents the hrGFP fluorescence intensity of the cell and was termed 'GFP intensity'. This GFP intensity is a relative value depending on the equipment.

2.3 Electrophysiological measurements

It is well known that prestin-expressing cells exhibit voltage-dependent nonlinear membrane capacitance against membrane potential. This nonlinear membrane capacitance reflects the charge movements across the plasma membrane of the cell due to prestin. To evaluate the expression level of prestin in prestin-expressing CHO cells, the membrane capacitance of each target cell was measured by the whole-cell patch-clamp method just after its fluorescence image was taken.

Measurements of membrane capacitance were conducted according to the previously reported procedure (see Ref. (12)) using the 'membrane test' feature of pCLAMP 8.0 acquisition software (Axon Instruments, Foster City, CA). Measurements were continuously repeated three times, and when maximum variations of membrane capacitance at each membrane potential obtained from three sequential measurements were 2% or less, the obtained data were used for the following analysis.

After the measurements, the values of membrane capacitance were plotted against membrane potential and fitted to the derivative of a Boltzmann function,

$$C_m(V) = C_{lin} + \frac{Q_{max}}{\alpha e^{\frac{V-V_{1/2}}{\alpha}}\left(1+e^{-\frac{V-V_{1/2}}{\alpha}}\right)^2}, \quad (2)$$

where C_{lin} is linear capacitance, Q_{max} is maximum charge transfer, V is membrane potential, $V_{1/2}$ is the voltage at which the maximum charge is equally distributed across the membrane and $\alpha = kT/ze$ is the slope factor of the voltage dependence of the charge transfer where k is Boltzmann's constant, T is absolute temperature, z is valence and e is electron charge. Fitting was performed using the Levenberg-Marquardt method.

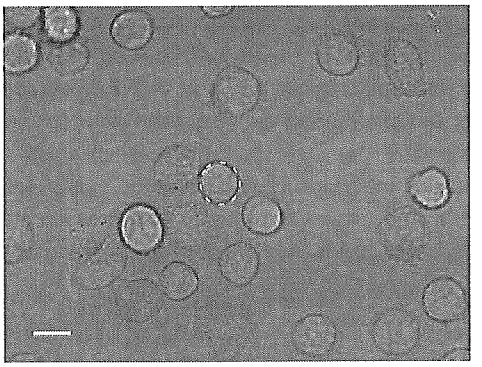

(a)

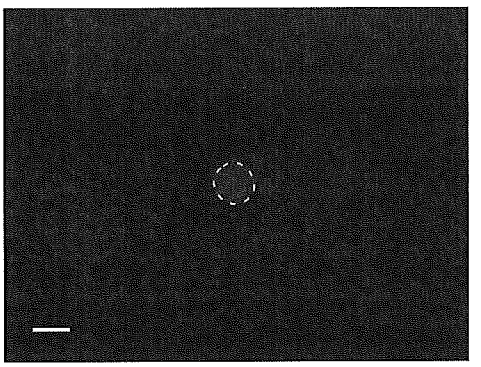

(b)

Fig. 5 Determination of an outline of the target cell. (a) Bright field image of prestin-expressing CHO cells. (b) Fluorescence image taken in the same frame as (a) under blue light (450–490 nm) exposure. Scale bars are 10 μm. The target cell was made identifiable by outlining it with the dashed circular curve in (a). Using the image in (b), the average intensity of pixels within the determined outline of the cell in (a) was calculated.

As Q_{max} is the total amount of charge transferred by prestin and e is electron charge, which equals the charge transferred by one prestin molecule, the number of prestin molecules in the cell is given by Q_{max}/e. As C_{lin} expressed in picofarads indicates the total capacitance of the plasma membrane of the cell, and the membrane capacitance of the cell per unit surface area is known to be 0.01 pF/μm^2[14], the surface area of the cell is expressed by $C_{lin}/0.01$ μm^2. The expression level of prestin per unit surface area, i.e., charge density, of the cell is therefore obtained from

$$\text{Charge density} = \frac{Q_{max}}{e} \Big/ \frac{C_{lin}}{0.01}. \quad (3)$$

3. Results

3.1 Relationship between average intensity of pixels and incoming light intensity

The obtained relationship between average intensities of pixels and relative incoming light intensities controlled by ND filters is shown in Fig. 6. The solid line represents the regression line obtained by the least squares method. The correlation coefficient was above 0.99. This result indicates that the calculated average intensity of pixels and the light intensity entering the object lens are in proportion.

3.2 Time dependence of fluorescence decay

To examine the time dependence of fluorescence decay[15] of the object cells, GFP intensity was measured every one second in the same frame ($n = 10$). Normalized GFP intensity, which was obtained from GFP intensity at each second divided by the initial GFP intensity, was plotted against exposure time to excitation light (Fig. 7). The result shown in Fig. 7 indicates that GFP intensity decreases to 30% of the initial GFP intensity with 20-second exposure to excitation light. As exposure to excitation light reduces fluorescence intensity, to obtain sharp photographs, the time interval between the start of exposure to excitation light and the capture of images should be shortened. In this study, this time interval was 1–2 seconds because it takes that long to set the optical path and capture an image.

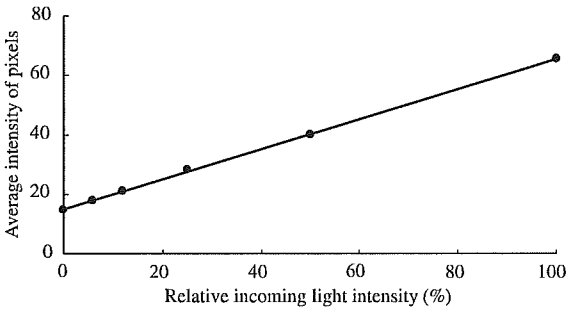

Fig. 6 Average intensities of pixels versus relative incoming light intensities. The solid line shows a linear fit to the data points using the least squares method. The correlation coefficient is above 0.99. This result indicates that the average intensity of pixels is proportional to the intensity of the incoming light.

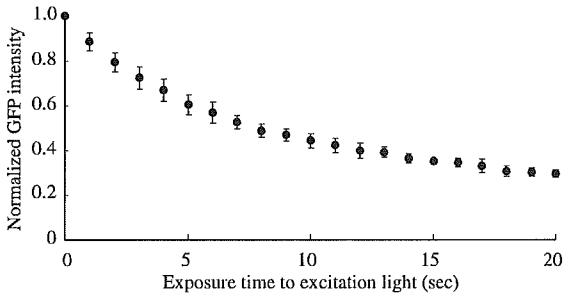

Fig. 7 Time course of fluorescence decay of hrGFP. GFP intensity was measured every one second and normalized by the initial GFP intensity ($n = 10$). GFP intensity was decreased to 30% of the initial GFP intensity by 20-second exposure to excitation light. Error bars show ±SD.

3.3 GFP intensity and charge density of prestin-expressing CHO cells

Representative data of the hrGFP fluorescence image, a brightness histogram of the pixels included within the outline of the target cell and measured membrane capacitance against membrane potential of the target cell are shown in Fig. 8.

In a group of 20 cells, fitting parameters of C_{lin} = 18.6±5.5 pF, Q_{max} = 126.2±107.2 fC, α = 41.3±10.7 mV and $V_{1/2}$ = −57.9±13.2 mV, and charge density of 394±227 $e^-/\mu m^2$ were obtained from patch-clamp recordings (mean ± SD).

The obtained charge density was plotted against GFP intensity (Fig. 9). The regression line was calculated using the least squares method. The correlation coefficient obtained from least squares fit is 0.67. This correlation between charge density and GFP intensity is significant at the 0.05 level.

4. Discussion

The fitting parameters α and $V_{1/2}$ of Eq. (2), which reflect the characteristic properties of prestin, obtained from 20 cells, correspond well with findings of previous reports[10),(16)], supporting the validity of the measurements. The average value of charge density, i.e., 394 $e^-/\mu m^2$, obtained from 20 cells, is larger than that previously reported, i.e., 196 $e^-/\mu m^2$[12)]. In this study, cells showing bright fluorescence were selected, while the previous study, cells were chosen at random. It is therefore considered that the charge density of 394 $e^-/\mu m^2$ obtained in this study is not indicative of the average charge density of the whole group of prestin-expressing CHO cells.

Membrane capacitance of cells, which did not fluoresce, was also measured. However, those cells did not show voltage dependent nonlinear capacitance. These results indicate that prestin was not expressed or was only slightly expressed in the cells which did not fluoresce. These results agree with the fact that there is a correlation between GFP intensity and the expression level of prestin.

As shown in Fig. 9, it was clarified that there was a correlation between the GFP intensity and the expression level of prestin although the correlation coefficient was 0.67. This result indicates that the expression level of prestin can be estimated by using GFP intensity. The cells which show high GFP intensity should be selected when high prestin-expressing cells are required.

To obtain GFP intensity with less error, the time interval between the start of exposure to excitation light and

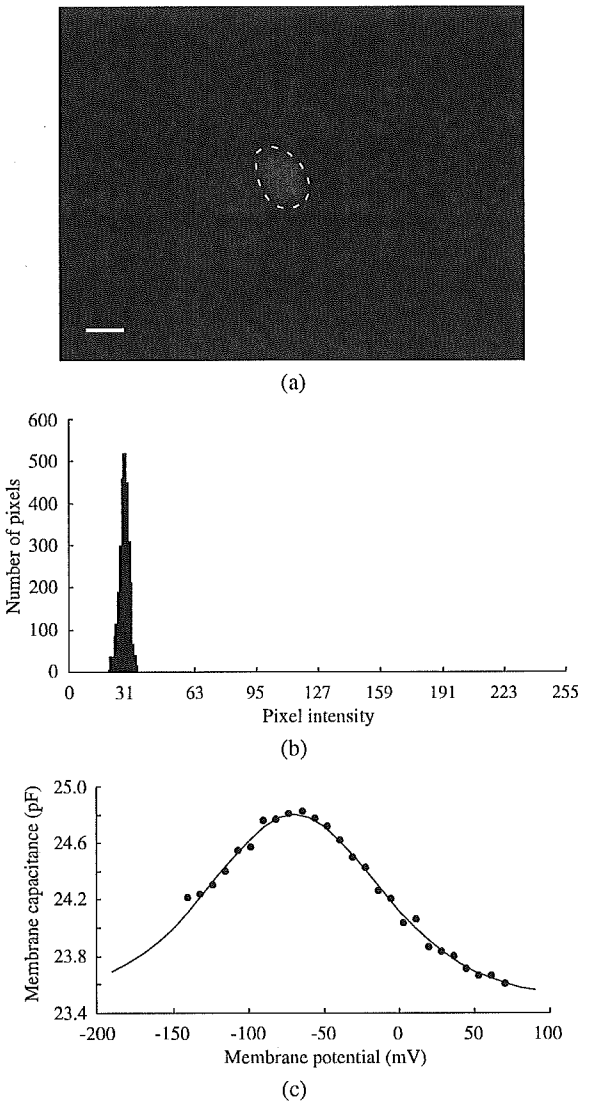

Fig. 8 Representative data of a prestin-expressing CHO cell. (a) hrGFP fluorescence image of a cell. The dashed circular curve is the outline of the target cell. Scale bar is 10 μm. (b) Brightness histogram of the target area. GFP intensity of the cell was determined to be 27.8. (c) Membrane capacitance versus membrane potential of the cell shown in (a). Data points were fitted with Eq. (2), which is shown by the solid line, with the following parameters: $C_{lin} = 23.4$ pF, $Q_{max} = 220.5$ fC, $\alpha = 40.7$ mV and $V_{1/2} = -71.7$ mV. Charge density of 589 $e^-/\mu m^2$ was obtained from these fitting parameters.

the capture of images should be the same because GFP intensity is reduced with time due to fluorescence decay (Fig. 7). In this study, however, the time interval between the start of exposure to excitation light and the capture of images ranged from one to two seconds. According to Fig. 7, there is a possibility that the obtained GFP intensity has a margin of error of up to 20%. Another way to reduce error is to apply a weaker excitation light and to improve

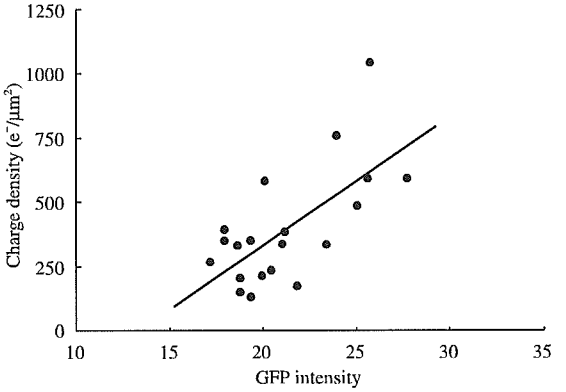

Fig. 9 Relationship between charge density and GFP intensity of prestin-expressing CHO cells. The solid line shows a linear fit to the data points using the least squares method. The correlation coefficient is 0.67. This relationship is significant at the 0.05 level. $n = 20$

the detection sensitivity of fluorescence because the application of weaker excitation light restricts the fluorescence decay.

5. Conclusions

It was demonstrated that hrGFP fluorescence intensity increases linearly as charge density increases. As charge density is proportional to the expression level of prestin, this result indicates that such expression can be evaluated by relative hrGFP fluorescence intensity in the constructed cell line.

Acknowledgements

This work was supported by a grant from the Human Frontier Science Program, by a Health and Labour Science Research Grant from the Ministry of Health, Labour and Welfare of Japan, and by Grant-in-Aid for Scientific Research on Priority Areas 15086202 from the Ministry of Education, Culture, Sports, Science and Technology of Japan.

References

(1) Davis, H., An Active Process in Cochlear Mechanics, Hear. Res., Vol.9 (1983), pp.79–90.
(2) Brownell, W.E., Bader, D. and Ribaupierre, Y., Evoked Mechanical Responses of Isolated Cochlear Outer Hair Cells, Science, Vol.227 (1985), pp.194–196.
(3) Dallos, P. and Evans, B.N., High-Frequency Motility of Outer Hair Cells and the Cochlear Amplifier, Science, Vol.267 (1995), pp.2006–2009.
(4) Kachar, B., Brownell, W.E., Altschuler, R. and Fex, J., Electrokinetic Shape Changes of Cochlear Outer Hair Cells, Nature, Vol.322 (1986), pp.365–368.
(5) Kalinec, F., Holley, M.C., Iwasa, K.H., Lim, D.J. and Kachar, B., A Membrane-Based Force Generation Mechanism in Auditory Sensory Cells, Proc. Natl. Acad. Sci. USA, Vol.86 (1992), pp.8671–8675.

(6) Santos-Sacchi, J. and Dilger, J.P., Whole Cell Currents and Mechanical Responses of Isolated Outer Hair Cells, Hear. Res., Vol.35 (1988), pp.143–150.
(7) Zenner, H.P., Motile Responses in Outer Hair Cells, Hear. Res., Vol.22 (1986), pp.83–90.
(8) Ashmore, J.F., A Fast Motile Response in Guinea-Pig Outer Hair Cells: The Cellular Basis of the Cochlear Amplifier, J. Physiol., Vol.388 (1987), pp.323–347.
(9) Zheng, J., Shen, W., He, D.Z.Z., Long, K.B., Madison, L.D. and Dallos, P., Prestin Is the Motor Protein of Cochlear Outer Hair Cells, Nature, Vol.405 (2000), pp.149–155.
(10) Ludwig, J., Oliver, D., Frank, G., Klöcker, N., Gummer, A.W. and Fakler, B., Reciprocal Electromechanical Properties of Rat Prestin: The Motor Molecule from Rat Outer Hair Cells, Proc. Natl. Acad. Sci. USA, Vol.98 (2001), pp.4178–4183.
(11) Liberman, M.C., Gao, J., He, D.Z.Z., Wu, X., Jia, S. and Zuo, J., Prestin Is Required for Electromotility of the Outer Hair Cell and for the Cochlear Amplifier, Nature, Vol.419 (2002), pp.300–304.
(12) Iida, K., Konno, K., Oshima, T., Tsumoto, K., Ikeda, K., Kumagai, I., Kobayashi, T. and Wada, H., Stable Expression of the Motor Protein Prestin in Chinese Hamster Ovary Cells, JSME Int. J., Ser. C, Vol.46, No.4 (2003), pp.1266–1274.
(13) Chalfie, M., Tu, Y., Euskirchen, G., Ward, W.W. and Prasher, D.C., Green Fluorescent Protein as a Marker for Gene Expression, Science, Vol.263 (1994), pp.802–805.
(14) Neher, E. and Marty, A., Discrete Changes of Cell Membrane Capacitance Observed under Conditions of Enhanced Secretion in Bovine Adrenal Chromaffin Cells, Proc. Natl. Acad. Sci. USA, Vol.79 (1982), pp.6712–6716.
(15) Swaminathan, R., Hoang, C.P. and Verkman, A.S., Photobleaching Recovery and Anisotropy Decay of Green Fluorescent Protein GFP-S65T in Solution and Cells: Cytoplasmic Viscosity Probed by Green Fluorescent Protein Translational and Rotational Diffusion, Biophys. J., Vol.72 (1997), pp.1900–1907.
(16) Oliver, D., He, D.Z.Z., Klöcker, N., Ludwig, J., Schulte, U., Waldegger, S., Ruppersberg, J.P., Dallos, P. and Bernd, F., Intracellular Anions as the Voltage Sensor of Prestin, the Outer Hair Cell Motor Protein, Science, Vol.292 (2001), pp.2340–2343.

Available online at www.sciencedirect.com
SCIENCE DIRECT®
Hearing Research 192 (2004) 57–64
HEARING RESEARCH
www.elsevier.com/locate/heares

Mechanical properties of sensory and supporting cells in the organ of Corti of the guinea pig cochlea – study by atomic force microscopy

Michiko Sugawara, Yuya Ishida, Hiroshi Wada *

Department of Bioengineering and Robotics, Tohoku University, Aoba-yama 01, Sendai 980-8579, Japan

Received 30 June 2003; accepted 20 January 2004
Available online 5 March 2004

Abstract

Mammalian hearing is refined by amplification of the motion of the cochlear partition. To understand the cochlear amplification, mechanical models of the cochlea have been used. When the dynamic behavior of the cochlea is analyzed by a model, elastic properties of the cells in the organ of Corti must be determined in advance. Recently, elastic properties of outer hair cells (OHCs) and pillar cells have been elucidated. However, those of other cells have not yet been clarified. Therefore, in this study, using an atomic force microscope (AFM), elastic properties of Hensen's cells, Deiters' cells and inner hair cells (IHCs) in the apical turn and those in the basal and second turns were estimated. As a result, slopes indicative of cell elastic properties were $(8.9 \pm 5.8) \times 10^3$ m^{-1} for Hensen's cells ($n = 30$), $(5.5 \pm 5.3) \times 10^3$ m^{-1} for Deiters' cells ($n = 20$) and $(3.8 \pm 2.6) \times 10^3$ m^{-1} for IHCs ($n = 20$), and Young's modulus were 0.69 ± 0.45 kPa for Hensen's cells and 0.29 ± 0.20 kPa for IHCs. There was no significant difference between elastic properties of each type of cell in the apical turn and those in the basal and second turns. However, it was found that there is a significant difference between Young's moduli of cells estimated in this study and those of the OHCs and pillar cells reported previously.

Keywords: Hensen's cells; Deiters' cells; Inner hair cells; Mechanical properties; Atomic force microscopy

1. Introduction

The mammalian ear has is characterize by sensitivity, broad dynamic range and sharp tuning. These characteristics are based on cochlear amplification, which is believed to be dependent on the voltage-dependent electromotile response of the outer hair cells (OHCs) in the organ of Corti (Brownell et al., 1985; Kachar et al., 1986). To understand cochlear amplification fully, it is necessary to characterize the role played by the involved components, namely, the basilar membrane, tectorial membrane and the organ of Corti containing OHCs, inner hair cells (IHCs), Deiters' cells, Hensen's cells, pillar cells and so on. For that purpose, mechanical models of the cochlea have been developed and evaluated (Kolston and Ashmore, 1996; Kolston, 1999; Steele, 1999; Bonke and Arnold, 1999), because direct observation of mechanical motion within the organ of Corti in vivo is currently difficult due to the extreme vulnerability of the cochlear amplifier to surgical insult. However, most of the mechanical properties of the cells in the organ of Corti have not yet been clarified. Therefore, to understand the cochlea mechanics, the mechanical properties of the cells in the organ of Corti should be determined in advance.

Tolomeo and Holley (1997) conducted a study of elastic properties in isolated guinea pig outer pillar cells. Using a three-point bending test, Young's modulus of pillar cells was determined to be 2×10^6 kPa. Pillar cells possess a cytoskeleton composed of thousands of

* Corresponding author. Tel.: +81-22-217-6938; fax: +81-22-217-6939.
E-mail address: wada@cc.mech.tohoku.ac.jp (H. Wada).
Abbreviations: IHC, inner hair cell; OHC, outer hair cell; AFM, atomic force microscopy

0378-5955/$ - see front matter © 2004 Elsevier B.V. All rights reserved.
doi:10.1016/j.heares.2004.01.014

parallel, cross-linked microtubules and actin filaments. It is known that the mechanical properties of cells are regulated by the structure of the cytoskeleton of the cells. Recently, using the contact mode of an atomic force microscope (AFM), Sugawara et al. (2002) reported that Young's modulus of the OHCs in the apical turn was 2.0 ± 0.81 kPa, whereas that of the OHCs in the basal and second turns was 3.7 ± 0.96 kPa. The difference in Young's modulus of the OHCs in each turn of the cochlea might affect the dynamic behavior of the organ of Corti. However, elastic properties of other cells in the organ of Corti have not yet been clarified. Therefore, in this study, an attempt was made to estimate elastic properties of Hensen's cells, Deiters' cells and IHCs in the apical turn and those in the basal and second turns with an AFM.

2. Materials and methods

2.1. Cell preparation

Eighty-eight ears of guinea pigs weighing between 200 and 500 g were used. After the bulla had been opened, the cochlea was detached and transferred to an experimental bath (the major ions in the medium were NaCl, 140 mM; KCl, 5 mM; $CaCl_2$, 1.5 mM; $MgCl_2 \cdot 6H_2O$, 1.5 mM; HEPES, 5 mM; Glucose, 5 mM; pH 7.2; 300 mOsm). The bony shell covering the cochlea was removed and the apical, second and basal turns of the organ of Corti were gently scraped off from the basilar membrane, and Hensen's cells and Deiters' cells were isolated by gently pipetting the organ of Corti in the experimental bath. In the case of the isolation of IHCs, the organ of Corti was transferred to an enzymatic digestion medium which contained 1 ml of the experimental bath medium and 1 mg trypsin. After enzymatic incubation for 15 min, IHCs were isolated by gently pipetting the organ of Corti in the experimental bath. By means of these isolation procedures, cells from the apical turn and those from the basal and second turns were identified. All experiments were performed at room temperature. The care and use of the animals in this study were approved by the Institutional Animal Care and Use Committee of Tohoku University, Sendai, Japan.

2.2. Atomic force microscopy

AFM is a valuable tool for evaluating elastic properties under physiological conditions (Radmacher, 1997). In this study, in order to evaluate elastic properties of cells in the organ of Corti, AFM studies were performed with a commercial instrument (NVB100, Olympus), in which the AFM unit is mounted on an inverted microscope. A v-shaped silicon nitride cantilever (OMCL-TR400PSA-2, Olympus) with a spring constant of 0.02 N/m was used. The typical radius of curvature of the cantilever tip was less than 20 nm.

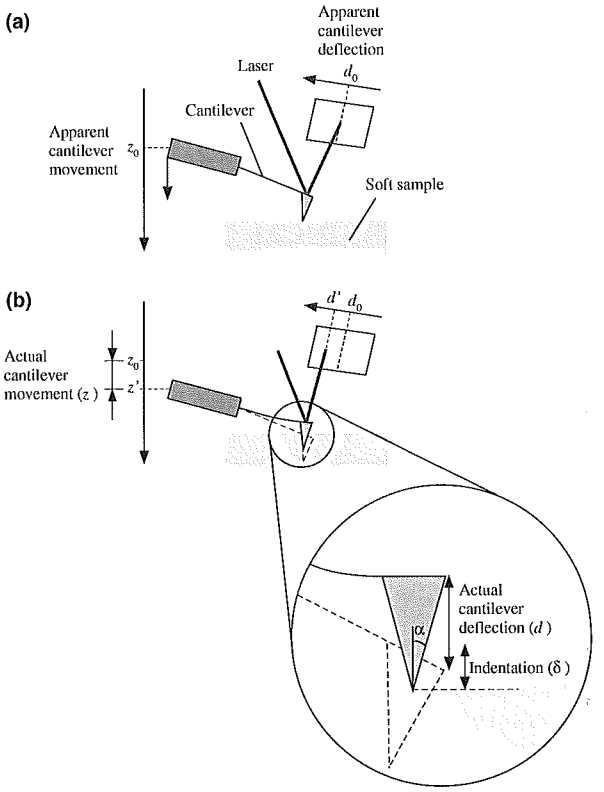

Fig. 1. Schematic of the cantilever on a soft sample. (a) Contact point – When the tip of the cantilever touches a sample, the apparent cantilever movement and the apparent cantilever deflection are defined as (z_0) and (d_0), respectively. (b) Indentation of the cell. When the cantilever is deflected, the actual deflection of the cantilever (d) is equal to ($d' - d_0$), where d' is the apparent cantilever deflection. Both (d') and (d_0) are detected by an optical detector which consists of a laser, a mirror and a photodiode array. At this stage, the actual movement of the cantilever (z) is equal to ($z' - z_0$), where (z') is the apparent cantilever movement. Indentation of the sample (δ) is given by $\delta = z - d$.

When the cantilever is moved by the piezoelectric scanner and the tip comes in contact with a sample, the cantilever is deflected (Fig. 1). The deflection of the cantilever is detected by an optical detector, in which a laser beam focused on the cantilever is reflected toward a photodiode array which acts as a position detector. Using this AFM system, a force curve which represents the relationship between the apparent cantilever deflection (d') and the apparent cantilever movement (z') caused by the piezoelectric scanner is obtained.

2.3. Analysis of the force curves

An example of the relationship between the apparent cantilever deflection (d') and the apparent cantilever

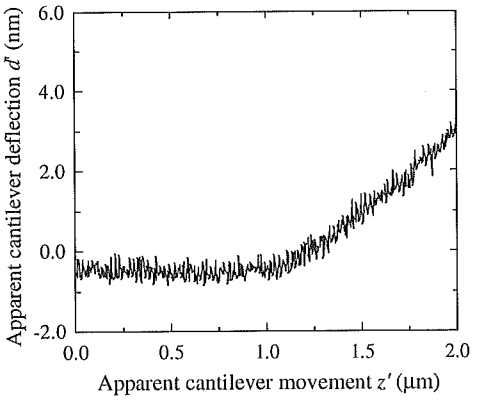

Fig. 2. Relationship between the apparent cantilever deflection (d') and the apparent cantilever movement (z') on the Hensen's cell.

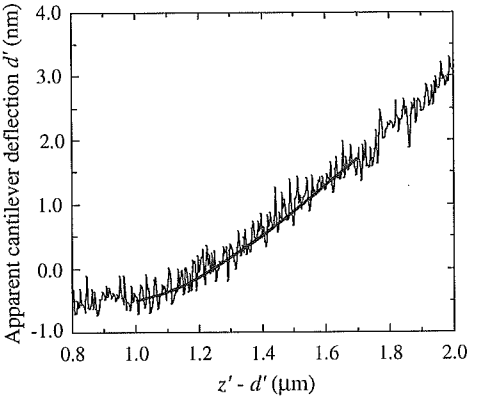

Fig. 3. Relationship between the apparent cantilever deflection (d') and the difference between the apparent cantilever deflection and the apparent cantilever movement ($z' - d'$) obtained from Fig. 2. By fitting this figure with Eq. (5) by the least squares method, the slope (a) is obtained. In addition, by comparing the slope (a) with $2E\tan\alpha/\pi k(1-\nu^2)$, Young's modulus is determined. Thin and thick lines represent the measurement data and the square regression line, respectively. In the analysis, Poisson's ratio was assumed to be 0.499, the half-opening angle and spring constant of the cantilever were 17° and 0.02 N/m, respectively, and Young's modulus was determined to be 0.26 kPa.

movement (z') on the Hensen's cell obtained from the AFM is shown in Fig. 2. Assuming that the contact point is (z_0, d_0) (Fig. 1(a)), the actual cantilever deflection (d) and the actual cantilever movement (z) can be written as follows:

$$d = d' - d_0, \tag{1}$$

$$z = z' - z_0. \tag{2}$$

As the difference between the actual cantilever movement (z) and the actual cantilever deflection (d) represents the sample indentation (δ) the indentation is given by

$$\delta = z - d, \tag{3}$$

which is shown in Fig. 1(b).

Several methods have been proposed to obtain the relationship between the cantilever deflection (d) and the sample indentation (δ). Sugawara et al. (2002) visually truncated the contact point and obtained the relationship between them. They then estimated the elastic properties of the sample by fitting the square regression line to this relationship. Some other researchers (Radmacher et al., 1996; Dimitriadis et al., 2002) proposed a method to determine the contact point together with the elastic properties of the sample numerically. As our previous method may possibly include some errors in determining the contact point, which could lead to incorrect elastic properties, in this study, an attempt was made to numerically determine the contact point together with the elastic properties.

Substituting Eqs. (1) and (2) into Eq. (3), the indentation is given by

$$\delta = z - d = (z' - d') - (z_0 - d_0). \tag{4}$$

From Fig. 2, the relationship between the apparent cantilever deflection (d') and the difference between the apparent cantilever deflection and the apparent cantilever movement ($z' - d'$) is obtained and shown in Fig. 3. It was possible to fit the curve in this figure with a square regression line given by

$$d' = a\{(z' - d') - b\}^2 + c, \tag{5}$$

and the parameters (a), (b) and (c) were obtained by the least squares method.

The parameter (a) is a representative of the elastic properties of the sample. When the tip of the cantilever comes in contact with a sample, the cantilever is deflected. If the sample is harder, the sample indentation is smaller and the cantilever deflection is larger, which leads to a larger slope in Fig. 1 and also in Fig. 2.

When the sample is elastic, isotropic and homogeneous and the tip is rigid and conical, the Hertz model, which describes the elastic response of a sample indented by the tip of the cantilever, is applied to the measurement data. When the tip is conical with a half opening angle (α), the relationship between the actual cantilever deflection (d) and the actual indentation (δ) is given by

$$d = \{2E\tan\alpha/\pi k(1-\nu^2)\}\delta^2, \tag{6}$$

where (k), (E) and (ν) represent the spring constant of the cantilever, Young's modulus of the sample and Poisson's ratio of the sample, respectively (Snedon, 1965; Wu et al., 1998). The substitution of Eqs. (2) and (4) into Eq. (6) results in the following equation:

$$d' = \{2E\tan\alpha/\pi k(1-\nu)^2\}\{(z' - d') - (z_0 - d_0)\}^2 + d_0. \tag{7}$$

The half-opening angle and the spring constant of the cantilever used in this experiment were 17° and 0.02 N/

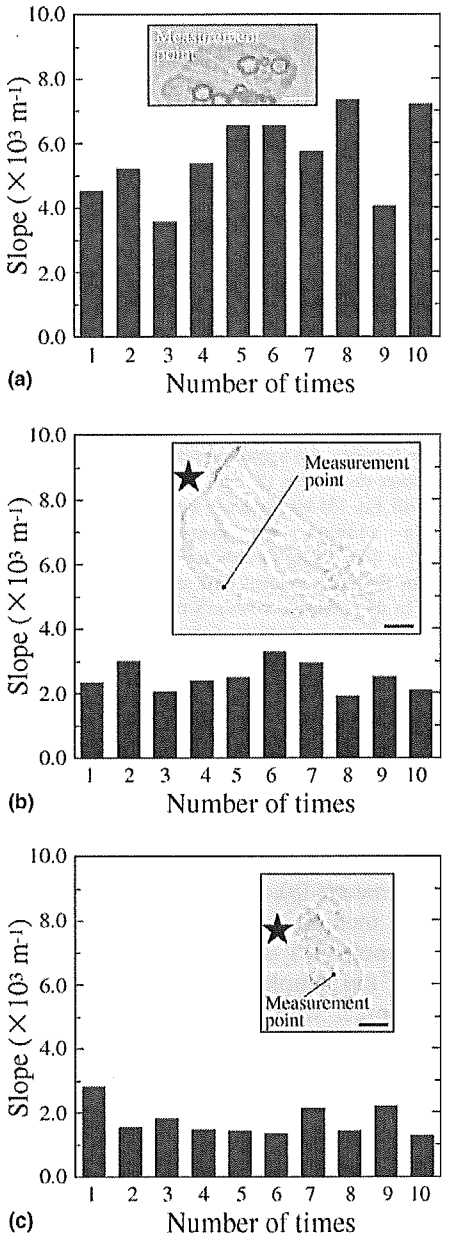

Fig. 4. The slopes calculated from the curves measured at the middle part of the cell. In this measurement, as the relationship between (d') and ($z' - d'$), which is shown in Fig. 3, was obtained 10 times at one point, the slope was calculated by fitting the relationship with a square regression line by the least squares method. (a) Hensen's cell – The mean slope is $(5.6 \pm 1.3) \times 10^3$ m^{-1} ($n = 10$). (b) Deiters' cell – The mean slope is $(2.5 \pm 0.44) \times 10^3$ m^{-1} ($n = 10$). (c) IHC – The mean slope is $(1.7 \pm 0.49) \times 10^3$ m^{-1} ($n = 10$). In each figure, an inset represents the measurement point on the cell. Bar = 10 μm. In (b) and (c), the star mark represents the side of the reticular lamina.

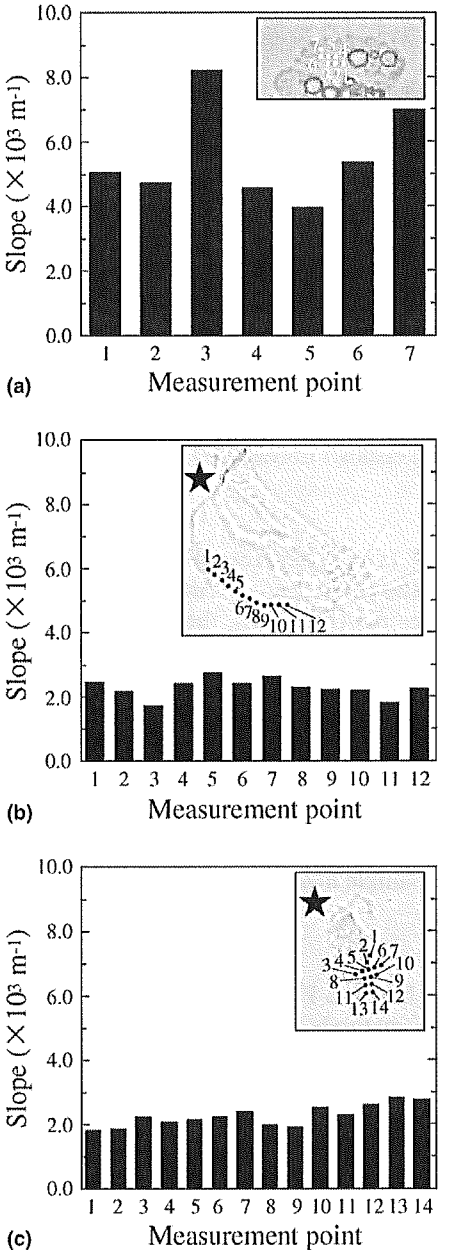

Fig. 5. The slopes calculated from the curves measured at several points on the cell. At each measurement point, the relationship between (d') and ($z' - d'$) was obtained five times, and the five slopes calculated from the relationships were averaged. (a) Hensen's cell – The mean slope is $(5.6 \pm 1.5) \times 10^3$ m^{-1}. (b) Deiters' cell – The mean slope is $(2.3 \pm 0.30) \times 10^3$ m^{-1}. (c) IHC – The mean slope is $(2.2 \pm 0.33) \times 10^3$ m^{-1}. In each figure, an inset represents measurement points on the cell, and the numbers in the inset correspond to those shown on the horizontal axis of the figure. In (b) and (c), the star mark represents the side of the reticular lamina.

m, respectively, and Poisson's ratio was assumed to be 0.499 since samples were biomaterials. When the Hertz model is applied to the analysis of the curve, as the slope (a) is equivalent to $2E \tan\alpha/\pi k(1 - \nu^2)$, with the parameters α, k and ν being given, Young's modulus (E) of the sample is estimated from this relationship. In addition, as the parameters (b) and (c) correspond to ($z_0 - d_0$) and (d_0), respectively, the contact point (z_0, d_0) is also determined.

2.4. Variance of slopes in the measurement

In this study, the noise in the recorded force curve caused variance of the slopes. Therefore, first, such variance was evaluated by obtaining the relationship between (d') and ($z' - d'$) 10 times at one point in the middle region of each cell and calculating the mean and standard deviation of the slope. The elastic properties of the nucleus might be greater than the other components of the cell's cytoplasm. Therefore, to avoid data scattering, measurements on the nuclei of Hensen's cells, Deiters' cells and IHCs were avoided. The results are shown in Fig. 4. Next, variance of the slopes caused by the differences in the locations of the measurement points was evaluated. At each measurement point, the relationship between (d') and ($z' - d'$) was obtained five times, and the five slopes calculated from the relationships were averaged. The results are shown in Fig. 5. In the measurement of OHCs, Sugawara et al. (2002) reported that the mean and standard deviation of the slope measured 10 times at one point in the middle region of an OHC and that measured at 21 points at intervals of 10 nm in the circumferential direction in the middle region of an OHC are $(7.6 \pm 0.37) \times 10^3$ m^{-1} ($n = 10$) and $(6.8 \pm 0.73) \times 10^3$ m^{-1} ($n = 10$), respectively. The latter variance is larger than the former one, which means that the slope obtained for an OHC depends on the location. On the other hand, comparison between Figs. 4 and 5 shows that the variance of the slopes due to the difference in the location of the measurement point in each cell is almost the same as that caused by the measurement 10 times at one point, i.e., the slope obtained for each cell is not dependent on the location of the measurement point. Therefore, to reduce the measurement time in this experiment, five force curves were obtained at one point, and the mean and standard deviation of the slopes were calculated for each cell.

3. Results

First, the relationships between the cantilever deflection and the indentation of Hensen's cells in the apical turn and those in the basal or second turns were measured. In this measurement, these relationships were not obtained for lipid droplets nor the nucleus in the cytoplasm, because the Hertz model is based on the assumption of the homogeneity of the sample. The fitting of square regression lines to the relationships between the cantilever deflection and the indentation of Hensen's cells led to estimates of the parameter a. The value obtained from the apical turn and that obtained in the basal turn or second turn were $(11.1 \pm 6.5) \times 10^3$ m^{-1} ($n = 15$) and $(6.8 \pm 4.2) \times 10^3$ m^{-1} ($n = 15$), respectively. There was no significant difference between the slope of Hensen's cells in the apical turn and that in the basal turn or second turn (Mann–Whitney test; $P < 0.05$), and the average of the slopes of the Hensen's cells in the basal, second and apical turns was $(8.9 \pm 5.8) \times 10^3$ m^{-1} ($n = 30$) (Table 1).

Next, the slopes of the Deiters' cells in the apical turn and those in the basal turn or second turn were estimated. In this measurement, the force curves of the Deiters' cells were obtained in the middle region, because that region is not on the nucleus nor on the phalangeal process which cannot be regarded as flat. The slope obtained from Deiters' cells in the apical turn and that in the basal turn or second turn were $(3.6 \pm 2.5) \times 10^3$ m^{-1} ($n = 10$) and $(7.3 \pm 6.7) \times 10^3$ m^{-1} ($n = 10$), respectively. There was no significant difference between the slope of Deiters' cells in the apical turn and that in the basal turn or second turn (Mann–Whitney test; $P < 0.05$), and the average of the slopes of the Deiters' cells in the basal, second and apical turns was $(5.5 \pm 5.3) \times 10^3$ m^{-1} ($n = 20$) (Table 1).

Finally, the slopes of the IHCs in the apical turn and those in the basal and second turns were estimated. In this measurement, ideally, the effect of trypsin on cells should have been evaluated before it was used for the isolation of the IHCs. However, as it was difficult to isolate IHCs without trypsin, this was not possible. On the other hand, OHCs can be isolated without trypsin. In addition, as OHCs have cytoskeletons which maintain the cell shape in vitro, it is considered that the effect of trypsin can be evaluated by examining the length change of the OHCs. Therefore, OHCs were incubated in an enzymatic digestion medium which contained 1 ml experimental bath medium and 1 mg trypsin for 30 min, and the length change of the OHCs during such incubation was measured. As a result, the mean value of the cell length after enzymatic incubation was found to be $98.4 \pm 1.4\%$ ($n = 10$), which was obtained by dividing the resulting cell length by the initial length. In addition, it is presumed that trypsin, which has a molecular weight of 23,300, cannot pass through the cell membrane. Therefore, its effect on the structure of IHCs might be negligible. In the measurement of the IHCs, as with the Hensen's cells and Deiters' cells, the force curves of the IHCs were obtained in the middle region, which is not on the nucleus. The slope obtained from the curve measured on IHCs in the apical turn and that in the basal turn or second turn were $(4.1 \pm 3.2) \times 10^3$ m^{-1}

Table 1
Slopes obtained on the cells in the organ of Corti

Cell	Slope ($\times 10^3$ m^{-1})	Number
Hensen's cell	8.9 ± 5.8	30
Deiters' cell	5.5 ± 5.3	20
IHC	3.8 ± 2.6	20

($n = 10$) and $(3.4 \pm 1.8) \times 10^3$ m^{-1} ($n = 10$), respectively. There was no significant difference between the slope of IHCs in the apical turn and that in the basal turn or second turn (Mann–Whitney test; $P < 0.05$), and the average of the slopes of the IHCs in the basal, second and apical turns was $(3.8 \pm 2.6) \times 10^3$ m^{-1} ($n = 20$) (Table 1).

4. Discussion

4.1. Young's modulus of cells

Using the AFM, the slopes of Hensen's cells, Deiters' cells and IHCs were estimated under physiological conditions. When the sample is elastic, isotropic and homogeneous, the Hertz model accurately describes the deflections measured in the AFM method, and Young's modulus may be estimated from the measured slopes. In the case of OHCs, when the cell's mechanical properties were evaluated by the AFM, both the orthotropic lateral wall and the isotropic cytoplasm were indented by the cantilever. As the thickness of the lateral wall is only 100 nm and the cytoplasm is much thicker than the lateral wall, the OHC can be assumed to be isotropic. However, in Deiters' cells, Slepecky and Chamberlain (1983, 1987) showed that microtubules run axially from the base of the cell close to the basilar membrane up to the reticular lamina. They also demonstrated that these microtubules exist not only at the lateral wall of the cell but also inside the cell. Therefore, it is presumed that Deiters' cells are anisotropic, and thus the Hertz model was not applied to the slopes of these cells. On the other hand, as both Hensen's cells and IHCs have no such structures as those seen in Deiters' cells, it is estimated that Hensen's cells and IHCs are isotropic. Therefore, Young's moduli were calculated from their slopes in Hensen's cells and IHCs, and were determined to be 0.69 ± 0.45 and 0.29 ± 0.20 kPa, respectively. They are shown in Table 2, together with the previously reported Young's moduli of the OHCs and pillar cells.

Young's moduli of various types of cells shown in Table 2 could be worthy of consideration. Firstly, comparison of Young's modulus of OHCs with those of Hensen's cells and IHCs shows that the former is larger than the latter, which suggests that the stiffness of OHCs is also greater. As the stiffness is directly related to the force produced by OHCs, i.e., the larger the stiffness, the larger the force, it is expected that OHCs are suitable for producing force in the organ of Corti. Secondly, comparison of Young's modulus of pillar cells with those of others shows that it is six orders of magnitude larger than any other cell type in Table 2. This result implies that the pillar cell can be considered to be a rigid structure when constructing a cochlear model.

4.2. Relationship between Young's modulus and the cell structure

Comparison of Young's moduli of Hensen's cells and IHCs obtained in this study with Young's modulus of OHCs reveals a significant difference (Mann–Whitney test; $P < 0.05$). In addition, Young's moduli of the cells obtained in this study were much smaller than that of the pillar cells (Table 2). From the evidence that the difference in elastic properties of the OHC in various parts of the cell is due to the difference in the cell structure, especially the difference in the number of filaments in the cell (Wada et al., 2003), one of the reasons for the difference in Young's moduli might be due to the difference in the cell structure. The OHC lateral wall consists of the plasma membrane, cortical lattice and subsurface cisternae (Holley and Ashmore, 1988). From immunological studies, the cortical lattice has been shown to be composed of a dense network of circumferential actin filaments and cross-linked spectrin (Holley and Ashmore, 1990; Holley et al., 1992; Nishida et al., 1993). These filaments are considered to be related to the elastic properties of the OHC. Pillar cells possess a cytoskeleton composed of thousands of parallel, cross-linked microtubules and actin filaments. Therefore, it is expected that these cells have a rigid structure. On the other hand, it has been confirmed that Hensen's cells consist of actin filaments and spectrin under the lipid bilayer (Slepecky et al., 1990; Mahendrasingam et al., 1998), and IHCs are known to consist of actin filaments, spectrin and microtubules under the lipid bilayer (Slepecky and Ulfendahl, 1992; Mahendrasingam et al., 1998). However, a cytoskeletal network as seen in the lateral wall of the OHC or in the pillar cell has not been confirmed in Hensen's cells and IHCs. Therefore, it is considered that the differ-

Table 2
Young's modulus of the cells in the organ of Corti

Cell	Young's modulus (kPa)	Number	References
Hensen's cell	0.69 ± 0.45	30	This study
IHC	0.29 ± 0.20	20	This study
OHC (in the apical turn)	2.0 ± 0.81	20	Sugawara et al. (2002)
OHC (in the basal and second turns)	3.7 ± 0.96	20	Sugawara et al. (2002)
Pillar cell	2×10^6		Tolomeo and Holley (1997)

ence between Young's moduli of Hensen's cells and those of IHCs obtained in this study and those of OHCs and pillar cells reported previously is due to the difference in the cell structure.

4.3. Difference in Young's modulus of the cell in each turn of the cochlea

Sugawara et al. (2002) reported that there is a significant difference between Young's moduli of the OHCs in the apical turn and that in the basal or second turns. As OHCs are constituents of the organ of Corti, a difference in the elastic properties of OHCs might affect the dynamic behavior of the organ of Corti along the length of the cochlea. As well as in the OHCs, significant differences between Young's modulus of Hensen's cells or IHCs in the apical turn and that in the basal or second turns were expected. However, no such significant differences were found. Taking only Young's modulus into consideration, this result implies that none of these cells affect the dynamic behavior of the organ of Corti along the length of the cochlea. However, there is another factor that has an effect on its dynamic behavior, that is, the shape of each cell which changes its mass.

It is known that there is a difference in the shape of Hensen's cells from turn to turn. The cells increase in size toward the apical turn (Santi, 1988). Such a difference in shape causes a difference in the mass of the cell. Therefore, it is suggested that variation in the local shape of the Hensen's cell is responsible, in part, for the variation in the dynamic behavior of the organ of Corti along the length of the cochlea. By contrast, the height of the cell body of the IHC, which has the shape of a flask with a diameter of about 9–13 μm at the widest point and a length of 20–25 μm (David et al., 2001), is fairly constant over the extent of the entire cochlea. Therefore, it is expected that the IHCs do not affect the dynamic behavior of the organ of Corti along the length of the cochlea.

5. Conclusions

In this study, the elastic properties of Hensen's cells, Deiters' cells and IHCs were estimated with an AFM. The results are as follows:

1. The slopes, which correspond to the elastic properties, of Hensen's cells, Deiters' cells and IHCs were $(8.9 \pm 5.8) \times 10^3$, $(5.5 \pm 5.3) \times 10^3$ and $(3.8 \pm 2.6) \times 10^3$ m^{-1}, respectively. There was no significant difference between elastic properties of the cells in the apical turn and those in the basal and second turns.
2. Young's moduli of Hensen's cells and IHCs were 0.69 ± 0.45 and 0.29 ± 0.20 kPa, respectively.
3. It was suggested that the difference between Young's moduli of the cells estimated in this study and those of OHCs and pillar cells reported previously is due to the difference in the cell structure.

Acknowledgements

The authors wish to thank Mr. A. Yagi, Olympus Optical Co., Ltd. and Mr. E. Imai, Olympus Promarketing, Inc., for technical assistance. This work was supported by a grant from the Human Frontier Science Program, by a grant from the Foundation Advanced Technology Institute, by a Health and Labour Science Research Grant from the Ministry of Health, Labour and Welfare of Japan, and by a Grant-in-Aid for Scientific Research (A) 11307033, a Grant-in-Aid for Scientific Research for Young Scientists (B) 13770947 and a Grant-in-Aid for Scientific Research on Priority Areas 15086202 from the Ministry of Education, Culture, Sports, Science and Technology of Japan.

References

Bonke, F., Arnold, W., 1999. 3D-finite element model of the human cochlea including fluid-structure couplings. ORL 61, 305–310.

Brownell, W.E., Bader, C.R., Bertrand, D., de Ribaupierre, Y., 1985. Evoked mechanical responses of isolated cochlear outer hair cells. Science 227, 194–196.

David, Z.Z.H., Zheng, J., Edge, R., Dallos, P., 2000. Isolation of cochlear inner hair cells. Hear. Res. 145, 156–160.

Dimitriadis, E.K., Horkay, F., Maresca, J., Kachar, B., Chadwick, R.S., 2002. Determination of elastic moduli of thin layers of soft material using the atomic force microscope. Biophys. J. 82, 2798–2810.

Holley, M.C., Ashmore, J.F., 1988. A cytoskeletal spring in cochlear outer hair cells. Nature 335, 635–637.

Holley, M.C., Ashmore, J.F., 1990. Spectrin, actin and the structure of the cortical lattice in mammalian cochlear outer hair cells. J. Cell Sci. 96, 283–291.

Holley, M.C., Kalinec, F., Kachar, B., 1992. Structure of the cortical cytoskeleton in mammalian outer hair cells. J. Cell Sci. 102, 569–580.

Kachar, B., Brownell, W.E., Altschuler, R., Fex, J., 1986. Electrokinetic shape changes of cochlear outer hair cells. Nature 322, 365–368.

Kolston, P.J., 1999. Comparing *in vitro*, *in situ*, and *in vivo* experimental data in a three-dimensional model of mammalian cochlear mechanics. Proc. Natl. Acad. Sci. USA 96, 3676–3681.

Kolston, P.J., Ashmore, J.F., 1996. Finite element micromechanical modeling of the cochlea in three dimensions. J. Acoust. Soc. Am. 99, 455–467.

Mahendrasingam, S., Furness, D.N., Hackney, C.M., 1998. Ultrastructural localisation of spectrin in sensory and supporting cells of guinea-pig organ of Corti. Hear. Res., 151–160.

Nishida, Y., Fujimoto, T., Takagi, A., Honjo, I., Ogawa, K., 1993. Fodrin is a constituent of the cortical lattice in outer hair cells of the guinea pig cochlea: Immunocytochemical evidence. Hear. Res. 65, 274–280.

Radmacher, M., 1997. Measuring the elastic properties of biological samples with the AFM. IEEE Eng. Med. Biol. Mag. 16, 47–57.

Radmacher, M., Fritz, M., Kacher, C.M., Cleveland, J.P., Hansma, P.K., 1996. Measuring the viscoelastic properties of human platelets with the atomic force microscope. Biophys. J. 70, 556–567.

Santi, P.A., 1988. Cochlear microanatomy and ultrastructure. In: Jahn, A., Santos-Sacchi, F. (Eds.), Physiology of the Ear. Raven Press, New York, pp. 173–199.

Slepecky, N., Chamberlain, S.C., 1983. Distribution and polarity of actin in inner ear supporting cells. Hear. Res. 10, 359–370.

Slepecky, N., Chamberlain, S.C., 1987. Tropomyosin co-localizes with actin microfimaments and microtubules within supporting cells of the inner ear. Cell Tissue Res. 248, 63–66.

Slepecky, N.B., Ulfendahl, M., 1992. Actin binding and microtubule-associated proteins in the organ of Corti. Hear. Res. 57, 201–215.

Snedon, I.E., 1965. The relation between load and penetration in the axisymmetric boussinesq problem for a punch of arbitrary profile. Int. J. Eng. Sci. 3, 47–57.

Steele, C.R., 1999. Toward three-dimensional analysis of cochlear structure. ORL 61, 238–251.

Sugawara, M., Ishida, Y., Wada, H., 2002. Local mechanical properties of guinea pig outer hair cells measured by atomic force microscopy. Hear. Res. 174, 222–229.

Tolomeo, J.A., Holley, M.C., 1997. Mechanics of microtubule bundles in pillar cells from the inner ear. Biophys. J. 73, 2241–2247.

Wada, H., Usukura, H., Sugawara, M., Katori, Y., Kakehata, S., Ikeda, K., Kobayashi, T., 2003. Relationship between the local stiffness of the outer hair cell along the cell axis and its ultrastructure observed by atomic force microscopy. Hear. Res. 177, 61–70.

Wu, H.W., Kuhn, T., Moy, V.T., 1998. Mechanical properties of L929 cells measured by atomic force microscopy: Effects of anticytoskeletal drugs and membrane crosslinking. Scanning 20, 389–397.